Supporting Information

Intrinsic-designed Polyimide Dielectric Materials with Large Energy Storage Density and Discharge Efficiency at Harsh Ultra-high Temperatures

Yaya Tian[a], Ming-Sheng Zheng[a,*], Yuchao Li[b,*], Chuqi Xu[c], Yiyi Zhang[c], Wei Liu[d], Zhi-Min Dang[e], Jun-Wei Zha[a,*]

[a] *Beijing Advanced Innovation Center for Materials Genome Engineering, School of Chemistry and Biological Engineering, University of Science & Technology Beijing, Beijing 100083, P. R. China*

[b] *School of Materials Science and Engineering, Liaocheng University, Liaocheng, 252059, P. R. China*

[c] *School of Electrical Engineering, Guangxi University, Nanning 530004, P. R. China*

[d] *School of Materials Science and Engineering, Nanchang Hangkong University, Nanchang 330063, P. R. China*

[e] *State Key Laboratory of Power System, Department of Electrical Engineering, Tsinghua University, Beijing 100084, P. R. China*

Corresponding to: *zhajw@ustb.edu.cn, zhengms@ustb.edu.cn, liyuchao@lcu.edu.cn*

Supporting Figures

Figure S1. (a) ^{1}H NMR and (b) ^{13}C NMR of the bis(2-cyano-4-nitrophenyl)amine; (c) The synthesis route of bis(2-cyano-4-nitrophenyl)amine and bis(2-cyano-4-aminophenyl)amine monomer; (d) ^{13}C NMR of the bis(2-cyano-4-aminophenyl)amine monomer.

Figure S2. The synthetic route of cyano-containing polyimides.

Figure S3. FTIR spectrum of the CPI films.

Figure S4. (a) DMA and (b)TGA curves of the CPI films.

Table S1. Thermal properties of the CPI films.

Figure S5. (a) Strain-stress and (b) Young modulus curves of the CPI films.

Table S2. Mechanical properties of the CPI films.

Figure S6. Frequency dependence of dielectric permittivity and loss of the CPI films at (a) R.T., (b) 50 ^{o}C, (c) 100 ^{o}C and (d) 150 ^{o}C.

Figure S7. Weibull plots of (a) Kapton PI at different temperatures; Comparison of the CPI films and Kapton PI at (b) 100 ^{o}C; (c) 150 ^{o}C; (d) 200 ^{o}C and (e) Comparison of E_b at different temperatures.

Figure S8. (a) Ultraviolet absorption spectra; (b) $(\alpha h\nu)^{0.5}$- $h\nu$ plots of CPI films.

Figure S9. Electric displacement-electric field (D-E) loops of (a) CPI-1, (b) CPI-2, (c) CPI-3 and (d) Kapton film at 25 ^{o}C.

Figure S10. Electric displacement-electric field (D-E) loops of (a) CPI-1, (b) CPI-2, (c) CPI-3 and (d) Kapton film at 150 ^{o}C.

Figure S11. Electric displacement-electric field (D-E) loops of (a) CPI-1, (b) CPI-2, (c) CPI-3 and (d) Kapton film at 250 ^{o}C.

Chemical structure and characterization of bis(2-cyano-4-nitrophenyl)amine and bis(2-cyano-4-aminophenyl)amine

^{1}H NMR (400 MHz, DMSO-d_6, δ): 10.37 (s, 1H), 8.78 (t, J = 2.1 Hz, 2H), 8.45 (dt, J = 9.3, 2.0 Hz, 2H), 7.49 (d, J = 9.2 Hz, 2H). ^{13}C NMR (400 MHz, DMSO-d_6, δ): 149.64, 142.14, 130.55, 129.58, 121.98, 115.45, 103.66.

^{1}H NMR (400 MHz, DMSO-d_6, δ): 7.49 (s, 1H), 6.79 (d, J = 9.0 Hz, 4H), 6.70 (d, J = 8.9 Hz, 2H), 5.18 (s, 4H). ^{13}C NMR(400 MHz, DMSO-d_6, δ): 145.9, 139.6, 124.5, 123.0, 118.9, 106.0.

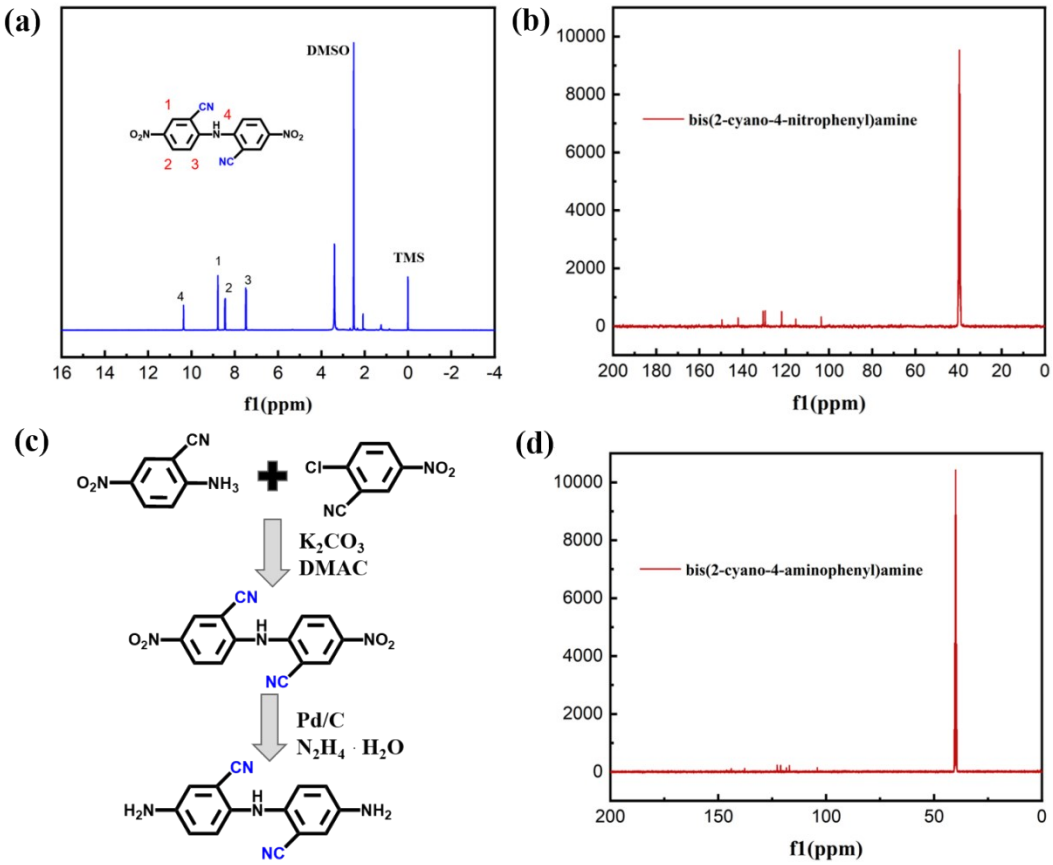

Figure S1. (a) ^{1}H NMR and (b) ^{13}C NMR of the bis(2-cyano-4-nitrophenyl)amine; (c) The synthesis route of bis(2-cyano-4-nitrophenyl)amine and bis(2-cyano-4-aminophenyl)amine monomer; (d) ^{13}C NMR of the bis(2-cyano-4-aminophenyl)amine monomer.

Chemical structure of the CPI films

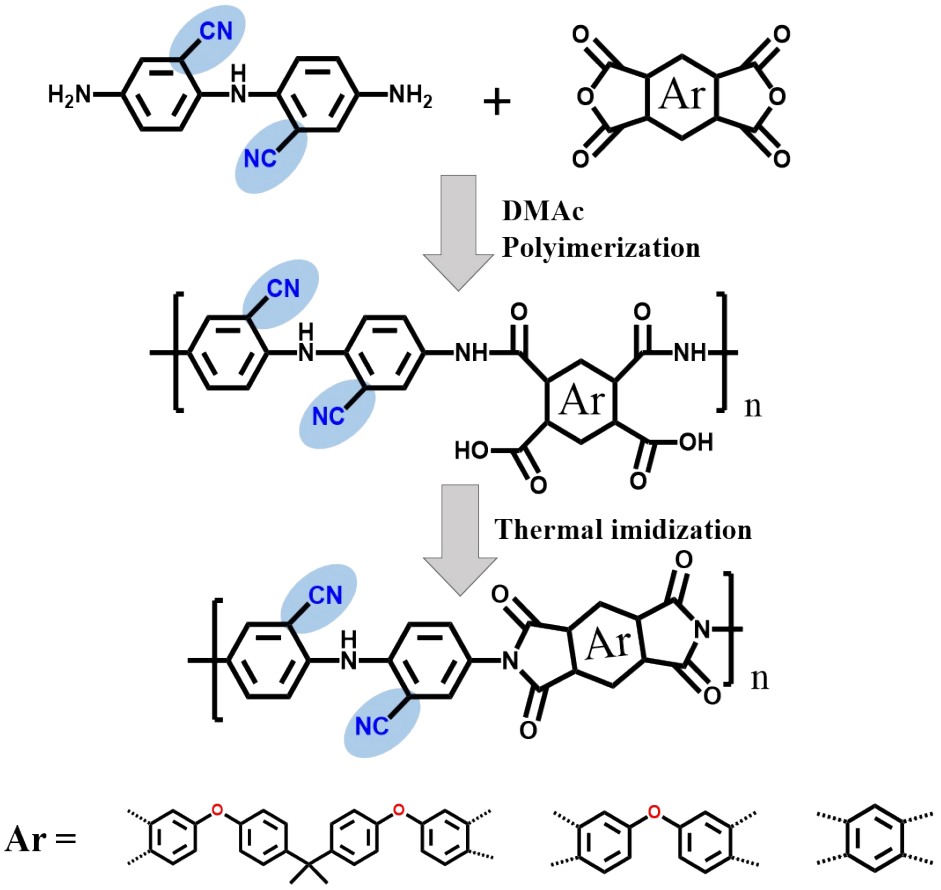

Figure S2. The synthetic route of cyano-containing polyimides.

FTIR spectra of the CPI films

The CPI-1 ~ CPI-3 films all have characteristic absorption peaks of polyimide structure: the characteristic absorption peak of -NH- at 1602 cm^{-1}, the characteristic absorption peaks of asymmetric and symmetric stretching vibration of the carbonyl group in the imide ring at 1780 cm^{-1} and 1727 cm^{-1}, the stretching vibration absorption peak of the -CN bond in the imide ring at 1375 cm^{-1}, and the characteristic absorption peak of -CN appear at 2218 cm^{-1}, respectively. It shows that the cyano group structure has been successfully introduced into the three CPI films.

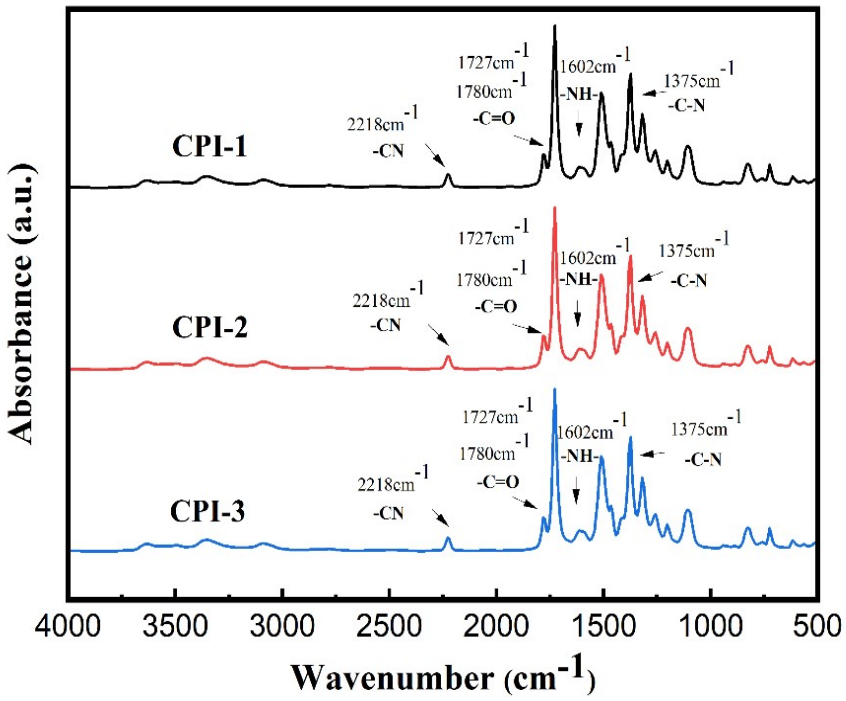

Figure S3. FTIR spectrum of CPI films.

Thermal properties of the CPI films

All CPI films exhibit excellent thermal stability with the decomposition temperature at 5% ($T_{d5\%}$) of 469-512 °C and decomposition temperature at 10% ($T_{d10\%}$) of 497-566 °C. Furthermore, the T_g of CPI films are of 262-400 °C due to the rigidity of polymer chains. Compared to CPI-1 and CPI-2 film, the CPI-3 film showed the highest T_g of 400 °C and excellent thermal stability. This is because of the rigid structure of PMDA and the strong π-π stacking between the polymer chains. The CPI-1 and CPI-2 films that both contain ether bonds have longer flexible segments, which are conducive to the movement of molecules, resulting in a lower T_g. Compared with the CPI-2 film, the CPI-1 film has a lower T_g value of only 242°C due to a longer flexible segment.

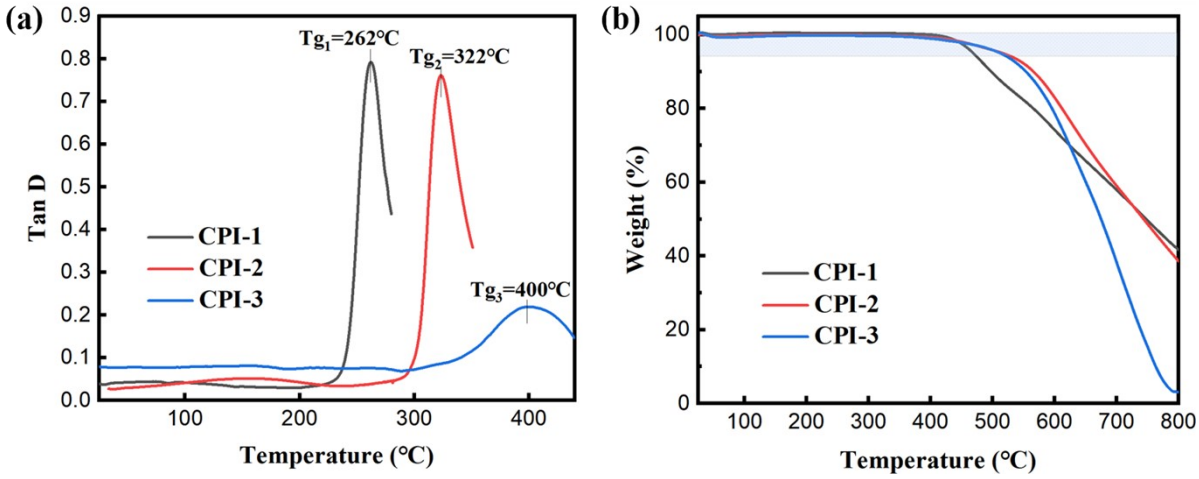

Figure S4. (a) DMA and (b) TGA curves of CPI films.

Table S1. Thermal properties of the CPI films

Samples	T_g [°C]	$T_{d5\%}$ [°C]	$T_{10\%}$ [°C]	T_{dmax} [°C]
CPI-1	262	469	497	593
CPI-2	322	516	566	620
CPI-3	400	512	553	697

Mechanical properties of the CPI films

The stress-strain curve of CPI films is shown in Figure S5. All CPI films exhibit excellent mechanical properties. The tensile strength of CPI-3 film is as low as 67.5 MPa, while the tensile strength of other PI films exceeds 100 MPa. The tensile modulus of all CPI films is greater than 4 GPa, and the maximum tensile modulus of CPI-3 film is 5.6 GPa. The elongation at break of all CPI films is between 11.0% and 12.8%. The CPI-3 film has good mechanical strength, which is mainly related to its rigid polymer chain structure.

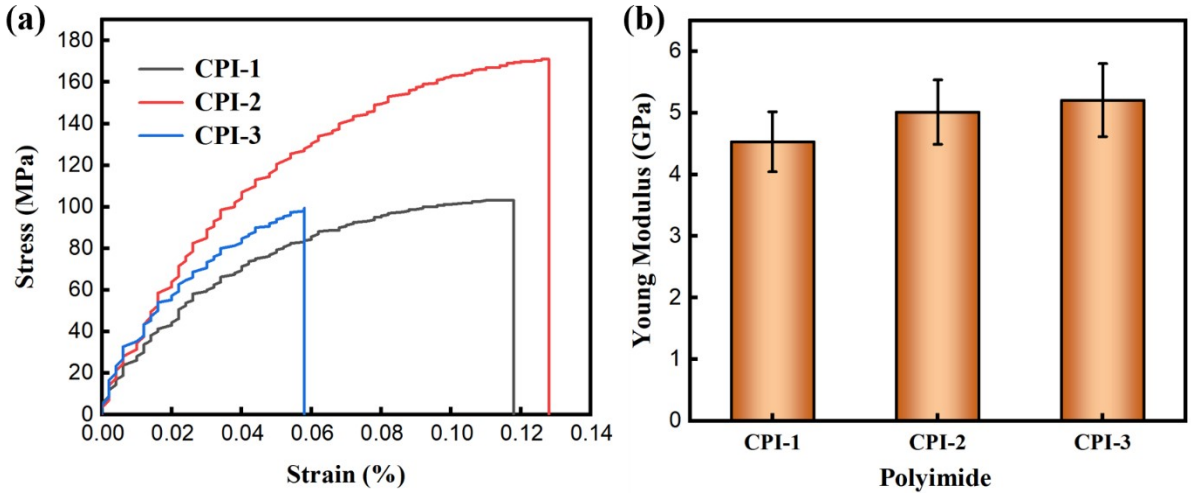

Figure S5. (a) Strain-stress and (b) Young modulus curves of the CPI films.

Table S2. Mechanical properties of the CPI films

Samples	Tensile Strength [Mpa]	Young's modulus [Gpa]	Elongation at break [%]
CPI-1	103	4.343	11.8
CPI-2	171	4.833	12.8
CPI-3	99	5.600	11.0

Dielectric properties of the CPI and Kapton PI films

The frequency dependence of dielectric permittivity and dielectric loss of the CPI films at different temperatures were investigated in the frequency range from 100 Hz to 10^6 Hz, as shown in Figure S6. It can be seen that at a given temperature, the dielectric permittivity of the three polyimide films shows a gradual decrease with the increase of frequency, but still have a good frequency stability. Farah Electronics pointed out that capacitors cannot be exposed to high temperature and high humidity for a long time. The suitable working environment needs to be -40~35 °C and the average humidity is less than 70%. Therefore, we further evaluated and compared the dependence of dielectric properties on temperature. The variable temperature dielectric was tested and compared between 25 °C and 150 °C. At the same frequency, the dielectric permittivity shows a downward trend with the gradual increase of temperature, while the overall trend does not decline too much.

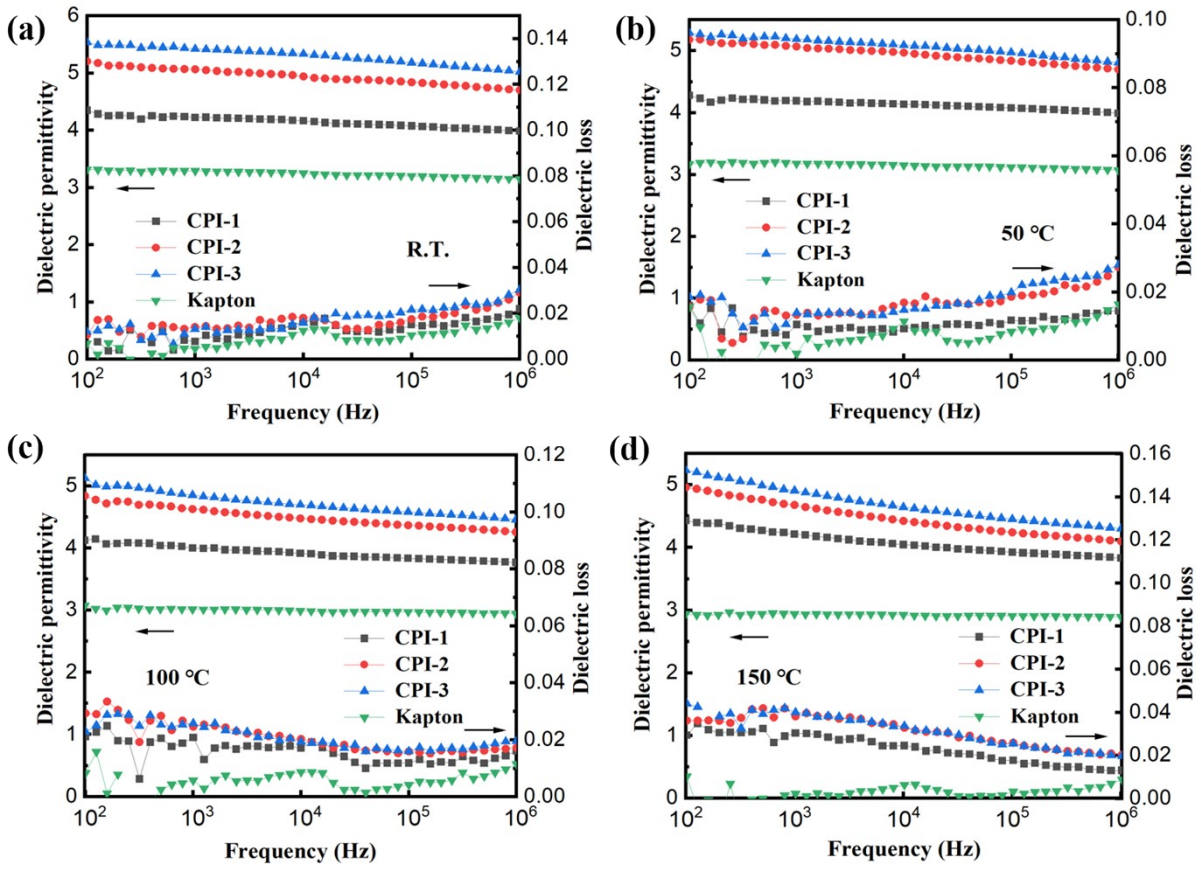

Figure S6. Frequency dependence of the dielectric permittivity and loss of CPI films at (a) R.T., (b) 50 °C, (c) 100 °C and (d) 150 °C.

The breakdown strengths at different temperatures and comparison values of CPI films and Kapton PI are shown in Figure S7. The breakdown strength (E_b) of the polymer at different temperatures is analyzed with a two-parameter Weibull statistic distribution function described as:

$$P(E) = 1 - exp[-(\frac{E}{E_b})^{\beta}]$$

where *P(E)* is the cumulative probability of electric failure, E is the measured breakdown field, Weibull breakdown strength E_b represents the field strength at the cumulative failure probability of 63.2%, and β is the shape parameter evaluating the scatter of the breakdown data. At least 15 measurements are made for each Weibull fitting.

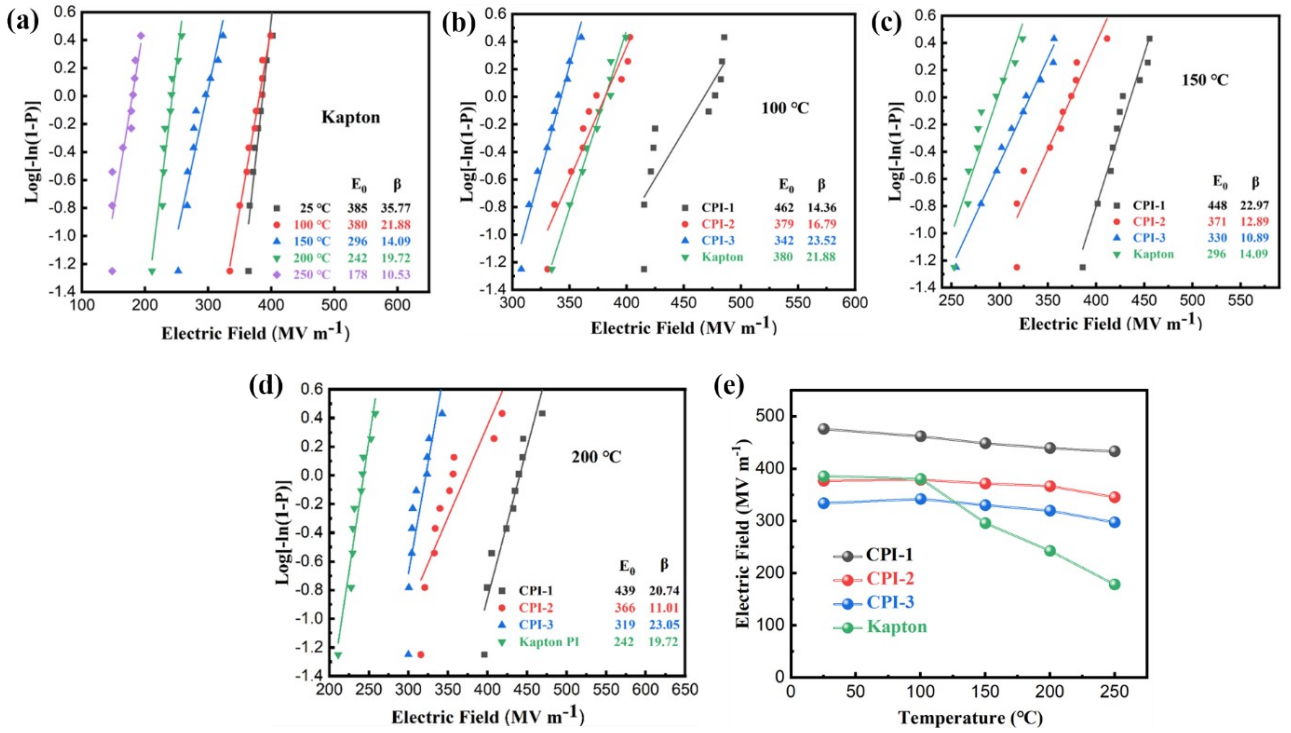

Figure S7. Weibull plots of (a) Kapton PI at different temperatures; Comparison of CPI films and Kapton PI at (b) 100 °C; (c) 150 °C; (d) 200 °C and (e) Comparison of E_b at different temperatures.

Band gaps of CPI films

Based on the UV absorption spectra (Figure S8a), the band gap of CPI films was estimated. The curve of $(\alpha h\nu)^{0.5}$ and $h\nu$ is converted from the Ultraviolet absorption spectra of the CPI films, where α is the absorption coefficient, h is the Planck's constant, and ν is the frequency of the incident photon. The band gap can be determined from the intercept of the plotted curve on $h\nu$ axis, as shown in Figure S8b.

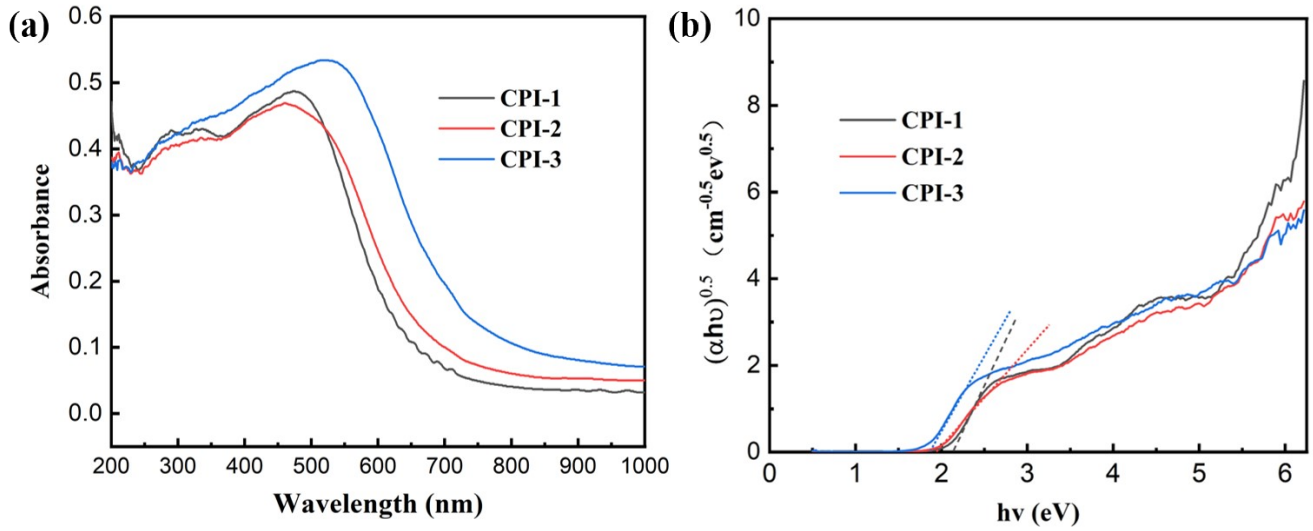

Figure S8. (a) Ultraviolet absorption spectra; (b) $(\alpha h\nu)^{0.5}$- $h\nu$ plots of CPI films.

***D-E* loops of CPI films and Kapton PI at different temperatures**

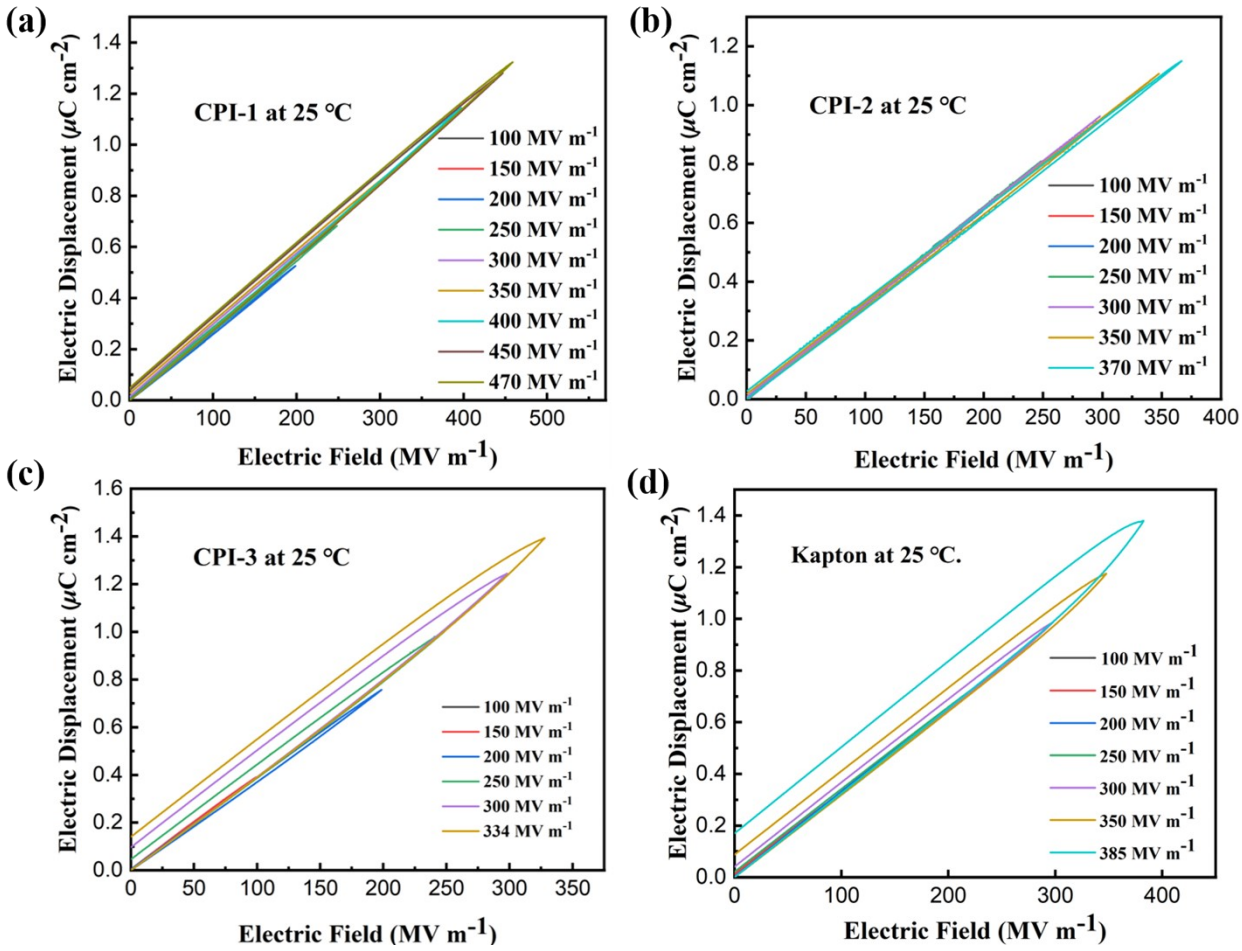

Figure S9. Electric displacement-electric field (D-E) loops of (a) CPI-1, (b) CPI-2, (c) CPI-3 and (d) Kapton film at 25 °C.

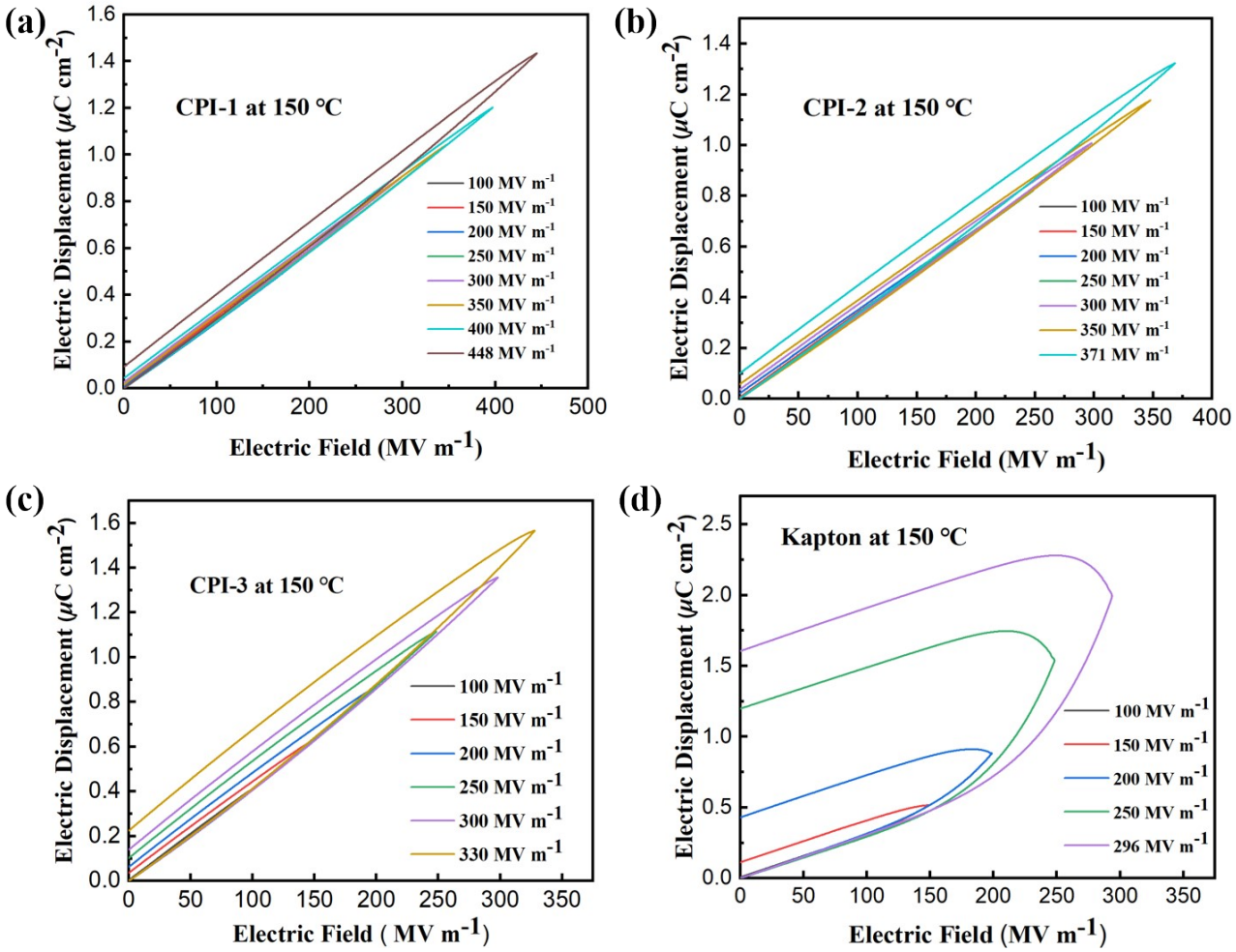

Figure S10. Electric displacement-electric field (D-E) loops of (a) CPI-1, (b) CPI-2, (c) CPI-3 and (d) Kapton film at 150 °C.

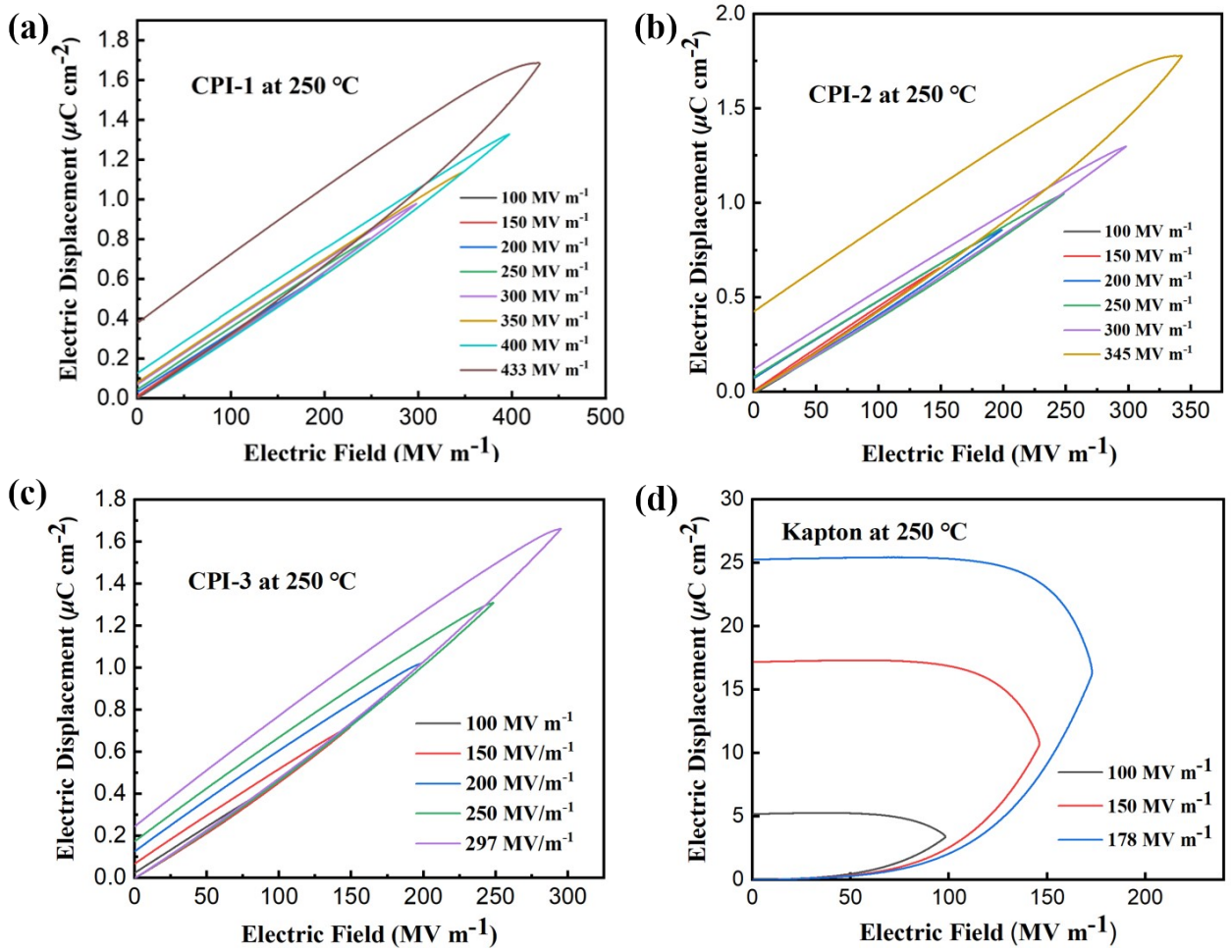

Figure S11. Electric displacement-electric field (D-E) loops of (a) CPI-1, (b) CPI-2, (c) CPI-3 and (d) Kapton film at 250 °C.